# LAMINAR-TO-TURBULENT TRANSITION IN A SHOCK-INDUCED SEPARATION BUBBLE

**L. Krishnan, N. D. Sandham**
Aeronautics and Astronautics
School of Engineering Sciences
University of Southampton, U.K, SO17 1BJ
krishnan@soton.ac.uk

**J. Steelant**
Aerothermodyanmcis Section (TEC-MPA)
ESTEC-ESA, The Netherlands

## ABSTRACT

Numerical simulations of the compressible Navier-Stokes equations are used to study laminar-to-turbulent transition in a separation bubble created by impingement of an oblique shock wave on a flat plate boundary layer at Mach 2. In contrast to separation bubbles in subsonic Mach numbers, steady laminar solutions are found, even for a strong pressure ratio ($p_3/p_1 = 1.91$) across the shock reflection. Such separation bubbles exhibit a multi-vortex recirculation zone. Using three-dimensional large eddy simulations with no upstream forcing a self-sustained transition process is observed, consistent with a change from convective to absolute instability of the two-dimensional solution. Additional simulations are carried out to study the development of the absolute instability, which initially involves spanwise distortion of vortex structures in the recirculation zone near reattachment. The pressure ratio for the onset of absolute instability is found to be between $p_3/p_1 = 1.50$ and 1.56. Bubble lengths are reduced when upstream forcing is applied.

## INTRODUCTION

Shock wave/boundary-layer interactions (SBLI) leading to flow separation are potentially damaging to the performance of supersonic flight vehicles. The extent of the separated region depends mainly on the strength of the incident shock wave and the nature of the boundary layer. A transitional/turbulent boundary layer offers more resistance to flow separation, while a laminar boundary layer separates even for moderate shock strengths, thus a thorough understanding of instability and transition to turbulence in shock-induced separation bubbles is very important. So long as the instability is convective in nature, the detached shear layer associated with a separation bubble acts as an amplifier of upstream flow disturbances. However, if the instability changes to absolute in nature it is possible that transition will occur independently of upstream disturbances. Instabilities associated with the incompressible laminar separation bubbles were studied in detail by Theofilis *et al.* (2000) and Alam & Sandham (2000), including discussions of the role of the percentage reverse flow in the change from convective instability (CI) to absolute instability (AI). For separation bubbles in supersonic external flow, as studied here, there is an additional simplification in that the free stream does not support upstream propagating waves and hence global modes based on a mechanism of downstream convecting instabilities and upstream propagating sound waves are less likely (some upstream acoustic propagation is possible through the separated flow region).

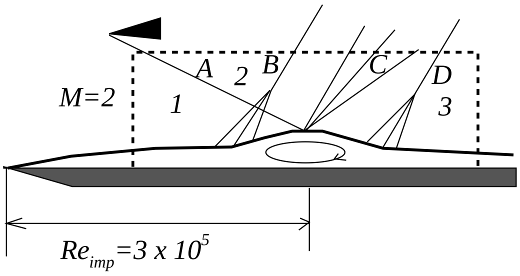


Figure 1: Schematic of the Sbli interaction; station 1 - upstream of the incident oblique shock (A), 2 - downstream of the incident oblique shock, 3 - downstream of the reattachment shock (D). B - separation shock, C - expansion waves. Dashed line is the present simulation domain.

Previous simulations of separation bubbles in supersonic flow include Katzer (1989), who performed 2D computations for various shock strengths ($p_3/p_1$ ranging from 1.2 to 1.5) and Shen et al. (2000) who found a secondary vortex within the separation bubble for shock strengths higher than 1.60. Referring to Figure 1 the strength of the interaction is denoted by the ratio of $p_3$ (the pressure downstream of the reflected shock) to $p_1$ (the pressure upstream of the interaction. Pagella *et. al.* (2002) studied the growth of small amplitude disturbances, while Chang and Malik (1994) found that the oblique mode of breakdown is the dominant transition mechanism in a low supersonic boundary layer flow. Recently, Yao et al (2007) studied the growth of small amplitude linear disturbances in a shock induced laminar separation bubble at Mach 2, 4.5 and 6.85 conditions. It was seen that transition at Mach 2 followed an oblique mode mechanism, while simulations at Mach 4.5 and 6.85 showed the prevalence of streamwise vortical structures rather than 2D Mack modes, which might have been expected to be active based on their local growth rates.

This paper is an extension of the Mach 2 case of Yao et al (2007), considering the effect of different strengths of interaction. Yao et al used $p_3/p_1 = 1.48$, which gave a bubble with $l_b/\theta_s = 563$, where $l_b$ is the length of the bubble and $\theta_s$ is the momentum thickness at the separation location. Thus at high shock strengths we are concerned mainly with the dynamics of separation bubbles ($l_b/\theta_s > O(10^3)$) induced by a strong impinging oblique shock wave. Firstly we consider a case of an interaction with $p_3/p_1$=1.91. Two-dimensional simulations are used to provide a base flow, which is then used as the starting point for three-dimensional large eddy simulations aimed at understanding the mechanism leading to a self-sustained transition, independent of upstream disturbances. Secondly we reduce the strength of the interaction to locate the point where the bubble changes from convective to absolute in character.

## SIMULATION DETAILS

The governing equations are discretised using a fourth-order central-difference scheme and the time integration is carried out using a third-order Runge-Kutta method. An artificial compression method (ACM) variant of a standard total variation diminishing (TVD) scheme is used to capture shock waves. The TVD is applied as a filter at the end of each full time step in the form of an additional numerical flux term. The present code also applies a Ducros (1999) sensor which takes low values where the flow is turbulent and values close to one in the vicinity of a shock. Selective filtering using a sixth-order centered explicit filter (Bogey and Bailly, 2004) is applied in the streamwise and the spanwise directions, where the grids are equally spaced, and is only needed when the present code is run using grids designed for large-eddy simulation (LES). In the present simulation it is applied after every 20 time steps with a small filtering coefficient of 0.03.

In flows with laminar-turbulent transition the LES subgrid scale (SGS) eddy viscosity must vanish in the laminar regions of the flow. In the case of the classic Smagorinsky model the SGS eddy viscosity does not vanish near the wall and also in the laminar regions. Proper near-wall scaling of the eddy viscosity therefore requires an additional damping function. With the basic Smagorinsky model, the model constant may also need to vary within the flow. Most of these difficulties are overcome when the dynamic Smagorinsky model is used, however the averaging procedure used to detemine the local model coefficient makes the model less suitable for use in transitional flows that may be highly intermittent. In the present study we use the mixed-time-scale (MTS) model of Inagaki et al. (2005) which requires no additional damping function or any averaging procedure. Inagaki et al. applied this model to prediction of various complex incompressible flows like plane channel flow, backward facing step flow, flow around a bluff body and flow around a circular cylinder. Krishnan and Sandham (2004) have previously used the MTS model for supersonic turbulent/transitional flows and found generally good agreement with the available data in the literature.

The flow domain is discretized using equally spaced grid points in the streamwise and spanwise directions and a stretched grid in the wall normal direction. The flow is assumed periodic in the spanwise direction, while no-slip and fixed-temperature conditions are applied at the flat plate surface. A characteristic non-reflective boundary condition and an integral boundary condition are used as outflow and top surface boundary conditions. Sutherland's law with a constant of $110K$ and a reference temperature of $288K$ is used to account for the variation of viscosity with temperature.

The present test case is similar to the early experiments of Hakkinen *et al.* (1959) and the recent LES study of Teramoto (2005). A schematic of the computational arrangement is shown in Figure 1; $p_1$ is the pressure before the interaction, $p_2$ is the pressure after the impinging shock and $p_3$ is the pressure after the interaction. The interaction itself includes a separation compression wave, an expansion as the flow turns over the top of the bubble and a further compression near the reattachment point. The shock is introduced by specifying the property jump conditions at the top boundary.

Table 1: Simulation details, $M_\infty = 2$,$T_w$=$1.68T_\infty$.

| Case | $Re_{\delta^*_{in}}$ | $L_x \times L_y \times L_z$ | $N_x \times N_y \times N_z$ |
|---|---|---|---|
| 2DS | 733 | $600 \times 110 \times 0$ | $401 \times 121 \times 0$ |
| 3DS | 733 | $600 \times 110 \times 15$ | $401 \times 121 \times 31$ |

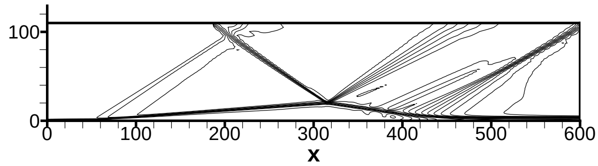


Figure 2: Iso-density contours showing the 2D SBLI interaction at Mach 2 with $p_3/p_1 = 1.91$.

All lengths are normalized by the inflow boundary-layer displacement thickness. Self-similar compressible laminar boundary layer relations are used to generate the Mach 2 inflow velocity and temperature profiles. The Reynolds number based on the inflow laminar boundary layer displacement thickness is 733 and $2.96\times10^5$ based on the distance from the leading edge to the shock impingement location (the same as Katzer (1989) and Teramoto (2005) and comparable to the $3.29 \times 10^5$ in Hakkinen et al. (1959).

To run the simulations, a steady laminar base flow is allowed to develop and then the shock conditions are imposed at the upper boundary. The 2D base flow solution is advanced in time until the change in the dimensions of the separation bubble is negligible (around 40 flow-through times).

## TWO DIMENSIONAL RESULTS FOR $P_3/P_1$=1.91

To begin we consider simulations of a strong interaction with $p_3/p_1 = 1.91$. Simulation details are presented in table 1 (case 2DS) and iso-contours of density are shown on Figure 2 to illustrate the main features of the flow. The impinging oblique shock wave is reflected as an expansion fan and the flow is deflected towards the wall downstream of the impinging location. Compression waves are seen near the separation and the re-attachment locations. The strong impinging shock creates a long separation bubble with $l_b/h_b = 23.30$ and $l_b/\theta_s = 1470$, where $h_b$ is the height of the bubble. The Reynolds number based on the bubble length is $Re_{lb} \approx 3 \times 10^5$. The separated region is found to have a multi-vortex structure with a large secondary bubble and a small tertiary bubble along the wall (Figure 3). Dilatational contours associated with these internal eddies are shown in (Figure 4). Figure 5 shows the streamwise velocity and sound speed distribution along the wall-normal direction at streamwise locations $x = 345$ and $x = 390$. At $x = 345$ the maximum reverse flow velocity is seen away from the wall and is about 20% of the free stream velocity at the inflow ($u_\infty$). Close to the re-attachment location

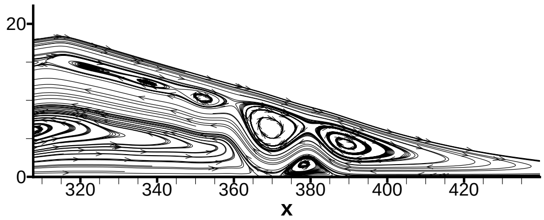


Figure 3: Separation bubble structure downstream of the shock impingement.

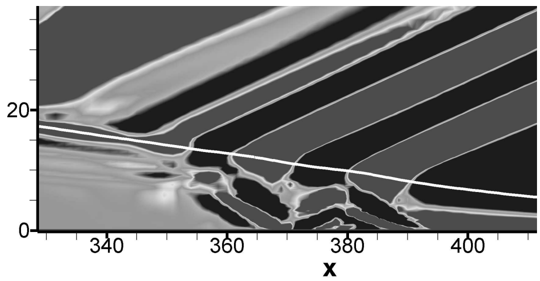


Figure 4: Dilatation contours showing the complex bubble structure. Dark colour negative dilatation value (Compression). white solid line - $M = 1$.

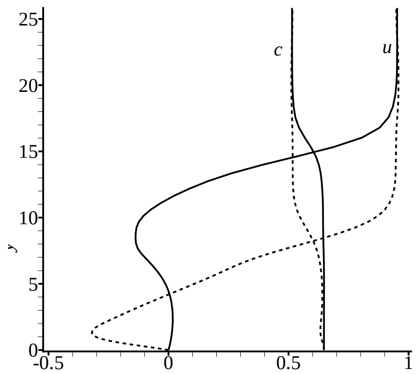


Figure 5: Wall-normal distribution of streamwise velocity ($u$) and sound speed ($c$) at $x = 345$ and $x = 390$.

($x = 390$) the reverse flow velocity increases to 32% $u_\infty$. At these locations the estimated convective Mach number ($M_c$) across the shear layer varies from 0.92 to 1.1.

Even though the bubble structure is complex, the unperturbed bubble is found to be steady in 2D simulations and there is no vortex shedding (even after 40 flow-through times). This is in contrast to low-speed simulations of 2D laminar separation bubbles where 2D shedding is commonly observed (Theofilis et al., 2000). The main difference here is that the external flow is supersonic, suggesting that upstream acoustic feedback may be a factor in simulations which have vortex shedding. Limited upstream propagation is possible through the separated flow and increasing the pressure ratio to $p_3/p_1 > 2.14$ did show vortex shedding with the present configuration.

For a shock strength of $p_3/p_1$=1.48 and $Re_{lb} = 200000$, Yao et al (2007) estimated amplification rates of the convectively unstable oblique mode disturbances to reach 'n-factor'

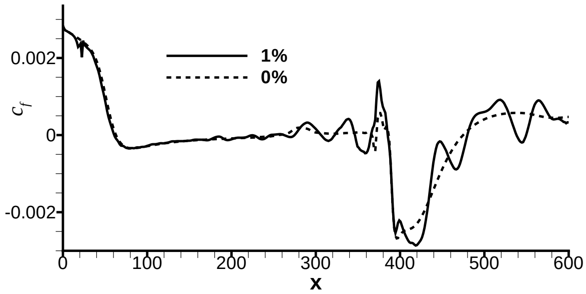


Figure 6: Skin friction ($c_f$) distribution along the flat plate for the 2D sbli with and without forcing.

value in the range 7-8. In the present work we tried to force vortex shedding at $p_3/p_1 = 1.91$ by introducing random disturbances at the wall ($20 < x < 23$) with disturbance amplitudes 0.1% (relative to the reference velocity at the inflow). There is no shedding observed with this disturbance. However, increasing the amplitude to 1% triggered shedding, as shown in the skin friction ($c_f$) distributions on Figure 6.

## LES OF TRANSITION IN THREE DIMENSIONS

In this section the 2D steady solution from the previous section (at $p_3/p_1 = 1.91$) is used as an initial condition for a 3D LES of transitional flow with random wall blowing/suction applied as a boundary condition upstream of the separation bubble ($20 < x < 23$). Grid details are given in Table 1 (case 3DS). First, a simulation with a disturbance amplitude of 0.1% relative to the inflow free stream value was carried out (the amplitude for which no shedding was observed in 2D). The simulation was run up to time $t$=1400 to allow the flowfield to develop. The second invariant ($\Pi$) of the velocity gradient tensor is used to identify flow structures and Figure 7 shows turbulent flow re-attaching to the wall with hairpin shaped structures downstream of the mean re-attachment location ($x_r = 413$). By comparison with the 2D simulations it is observed that at $M = 2$ the separated shear layers are much more unstable with respect to oblique modes than 2D modes (as in Yao et al).

Simulations with a higher amplitude of 8% and with no upstream forcing were carried out to investigate the sensitivity of the separation bubble to the forcing. With 8% forcing the bubble is found to shorten considerably in length, as seen in a plot of mean skin friction on figure 8, compared to the case with 0.1% perturbations and with the 2D solution. In this figure the mean span- and time-averaged statistics are averaged over 411 time units (after initial delay of 3-4 flow-through times to allow the flow to develop). Bubble length is taken as the distance from the first separation (skin friction crossing zero from positive to negative) to the final reattachment. The large amplitude disturbance is found to delay separation significantly, with transition occurring immediately downstream of the impinging oblique shock. With the disturbances turned off the transition process was observed to sustain itself with time, and not return to the steady 2D solution. This is in agreement with Teramoto et al (2005), and suggests that the self-sustained transition process has a physical origin.

The mean wall pressure distribution shown on Figure 9 shows a weak pressure plateau upstream of the impinging shock and a sharp pressure rise near re-attachment for the 8% random disturbance. The mean velocity profile at

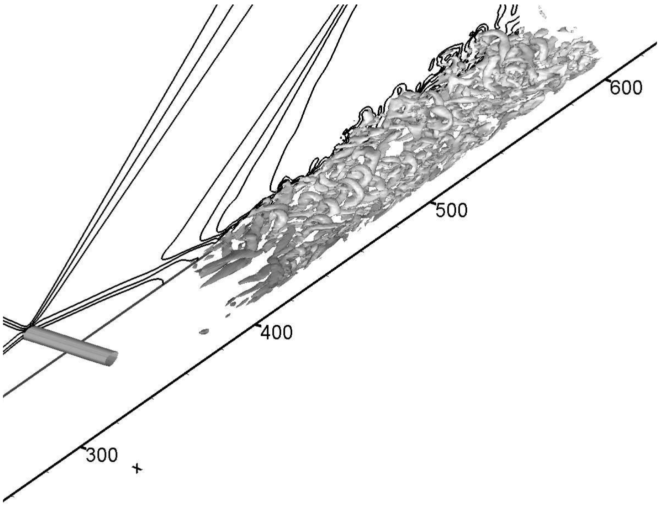


Figure 7: Second invariant of the velocity gradient tensor showing the coherent structures in the flow (-.001).

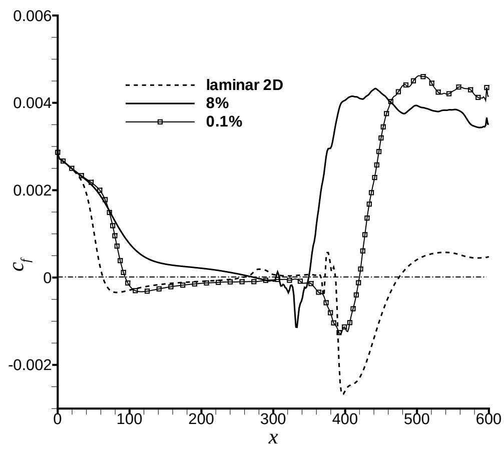


Figure 8: Mean skin friction distribution showing the effect of disturbance amplitude on the separation bubble.

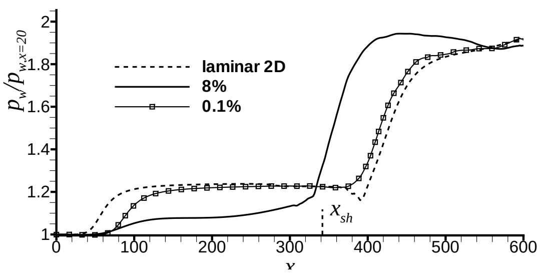


Figure 9: Mean wall static pressure distribution.

$Re_x = 4.75 \times 10^5$ indicates a well developed turbulent flow (Figure 10). A comparison of the rms velocity fluctuations with the incompressible boundary layer data of Spalart (1988) is given in Figure 11. Compared to the equilibrium boundary layer there are large overshoots near $y^+$=200, indicating a long relaxation process after the transition process. The estimated momentum thickness Reynolds number based on the properties at $Re_x = 4.75 \times 10^5$ is $Re_\theta = 2181$. The present grid resolution in viscous wall units based on

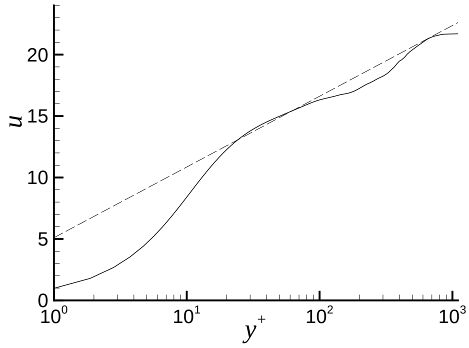


Figure 10: Mean velocity profile at $Re_x = 4.75 \times 10^5$ (solid line) compared to the log-law : $1.0/0.41\ ln(y^+) + 5.1$ (dashed line).

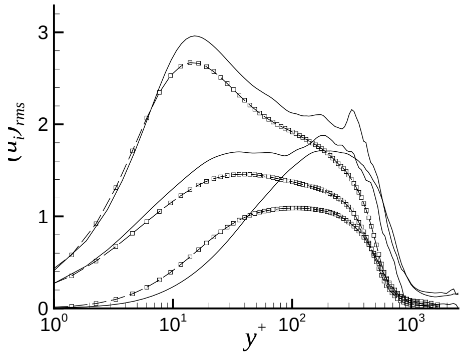


Figure 11: Rms velocity fluctuations at $Re_x = 4.75 \times 10^5$ (solid line) compared to Spalart (1988) incompressible turbulent boundary layer (dashed line with symbols). From top to bottom the curves correspond to $u', w', v'$.

maximum friction velocity at the wall are $\Delta x^+ = 33.95$, $\Delta y_1^+ = 0.93$, $\Delta z^+ = 22.63$. This is comparable to the LES of Teramoto (2005) with $\Delta x^+ = 33.4 - 70.2$, $\Delta y_1^+ = 0.7 - .74$, $\Delta z^+ = 9.7 - 28.1$.

## EVIDENCE FOR A LOCAL ABSOLUTE INSTABILITY

In this section we investigate the transition process in the absence of upstream forcing. Without initial forcing, any absolute instability would be fed only by numerical round-off errors. A more controlled method of checking for the presence of an absolute instability is to add a small amplitude random disturbance to the initial flow field and then integrate the flow forward in time, still without any upstream forcing. If the disturbances grow convectively, but gradually wash out of the computational domain, the flow can be said to be convectively unstable. However if growth is seen in time at a particular point in space the flow may be taken to be absolutely unstable. Therefore a 3D simulation was set up using the 2D steady flow solution and random noise with amplitude 0.1% was added to the flow field at time $t = 0$.

The time-dependent evolution of the 3D flow field is shown in Figure 12. Iso-contours of wall-normal vorticity are plotted (which is zero for the 2D steady flow solution). The random initial disturbance is found to generate growing oblique mode disturbances in the separated shear layer (Figure 12a, at $t = 340$), which is the most unstable region of such flows. Figure 12b at $t = 549$ shows how these oblique structures have convected downstream to the shock

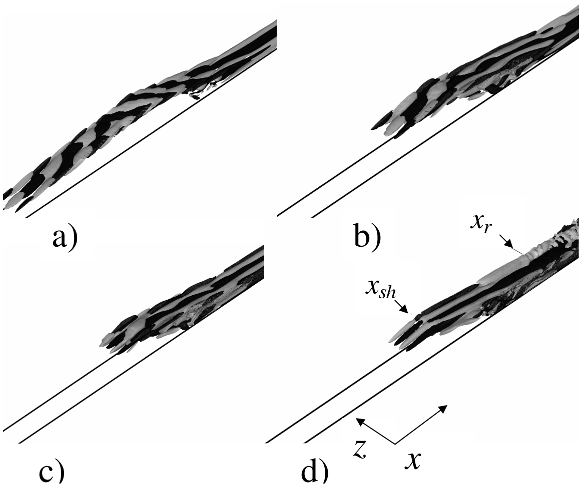


Figure 12: Iso-surfaces of wall-normal vorticity ($\omega_y$=+.001, -0.001) showing the temporal evolution of the flow; a) $t$ = 340, b) $t$ = 549, c) $t$ = 620, d) $t$ = 815.

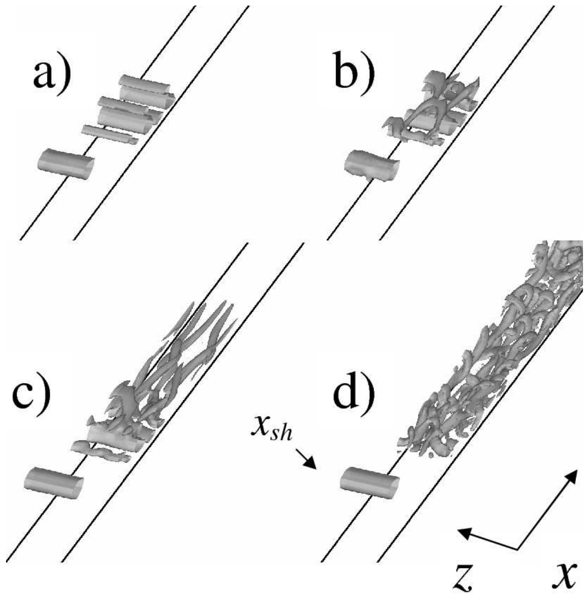


Figure 13: Iso-surface of second invariant (-0.001) showing the formation of coherent structures near the re-attachment location; a) $t$ = 340, b) $t$ = 549, c) $t$ = 620, d) $t$ = 815.

impingement location. Longitudinal structures are seen in Figure 12c-d before the flow becomes nonlinear downstream of reattachment. Chang and Malik (1994) and Sandham et al (1994) have also observed the evolution of longitudinal structures due to the interaction of two oblique modes with opposite signs and the convective phase of the current growth process appears similar here.

Three-dimensional iso-contours of the second invariant of the velocity gradient tensor are used to identify the flow structures associated with the transition process. At $t = 340$, spanwise coherent vortex structures associated with the steady separation bubble internal vortices are seen near the reattachment location (Figure 13a). The next stage of the process shows how these 2D structure have become distorted into a set of staggered $\Lambda$-shaped structures (Figure 13b-c). Finally, breakdown starts from the generation of hairpin-shaped turbulent structures in the flow (Figure 13d, $t = 815$). This process shows growth in time at a fixed spatial location (corresponding to the strongest internal vortices in the separation bubble) and implies the presence of an absolute instability.

To find the critical pressure ratio $p_3/p_1$ a series of simulations were conducted. Yao et al (2007) created a separation bubble with a shock strength $p_3/p_1 = 1.48$ and found the bubble to be absolutely stable. This suggest that at some point in between $1.48 < p_3/p_1 < 1.91$ the transition changes from a convectively unstable oblique-mode to an absolutely unstable mechanism. To investigate this, 3D simulations with an initial random disturbance of 0.1% were carried out for separation bubbles at $p_3/p_1 = 1.50, 1.56$ and 1.74. For these simulations, the spanwise width of the domain was doubled to $L_z = 30$ and the grid was changed to have $N_z = 61$ grid points. Both the $p_3/p_1 = 1.56$ and 1.74 cases showed non-linear breakdown to turbulence. The transitional structures during the early non-linear stage for $p_3/p_1 = 1.56$ are shown in Figure 14. Quasi-streamwise structures, staggered hairpin shaped structures and single-legged hairpin structures can be clearly identified in the flow downstream of the re-attachment location. The temporal evolution of the spanwise velocity amplitude for a selection of the present cases is shown in Figure 15. The order of magnitude change in amplitude from $p_3/p_1 = 1.50$ to $p_3/p_1 = 1.56$ is evidence for a sudden change to an absolutely unstable transition regime.

Figure 16 provides a summary of the laminar-turbulent transition in a separation bubble and the effect of upstream forcing on the length of a shock-induced separation bubble. Three key pressure ratios ($p_3/p_1$) are those for incipient laminar separation ($i_L$), for the change from convective to absolute instability ($i_{AI}$) and for incipient separation of an upstream turbulent boundary layer ($i_T$). For no upstream turbulence, increasing pressure ratio gives a solution which follows path (a) up to $i_{AI}$ and path (b) thereafter. A small decrease in bubble length is expected as $i_{AI}$ is crossed, due to more rapid reattachment of a turbulent shear layer. For increasing forcing amplitude the bubble length shrinks (case c), the incipient separation point may be postponed (case d) and, for sufficiently high forcing (case f), the bubble length may decrease below that obtained for a turbulent upstream boundary layer (case e). A hysteresis loop may be present near $i_{AI}$.

## SUMMARY

Two- and three-dimensional simulations have been used to elucidate the dynamics of transitional separation bubbles created in a Mach two boundary layer by impingement of an oblique shock wave. There are a number of differences in bubbles created in this way compared with transitional bubbles seen in low speed flows. Firstly, we find that in two-dimensions a steady solution can exist (at least for $p_3/p_1 < 1.91$), compared to subsonic bubbles where time-dependent vortex shedding is prevalent. As the shock strength is increased above that required for incipient separation, secondary and tertiary separations form and there is a change to multi-celled vortex structure within the separation zone. Secondly, it is seen that the steady separation bubble is most unstable to three-dimensional disturbances, with transition following an oblique mode breakdown process. As the upstream forcing amplitude is increased the bubble length reduces considerably. Thirdly, there is a change in the nature of the transition process from con-

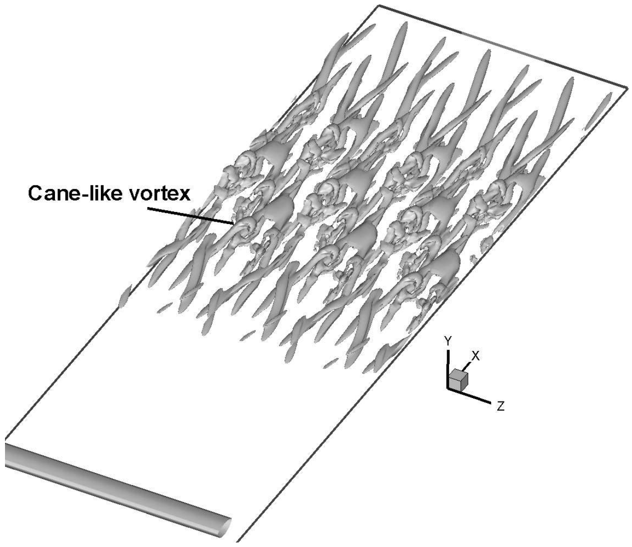


Figure 14: Second invariant showing the staggered transitional flow structures for the case with $p_3/p_1 = 1.5551$ at $t = 667$. Two periods repeated in the spanwise direction.

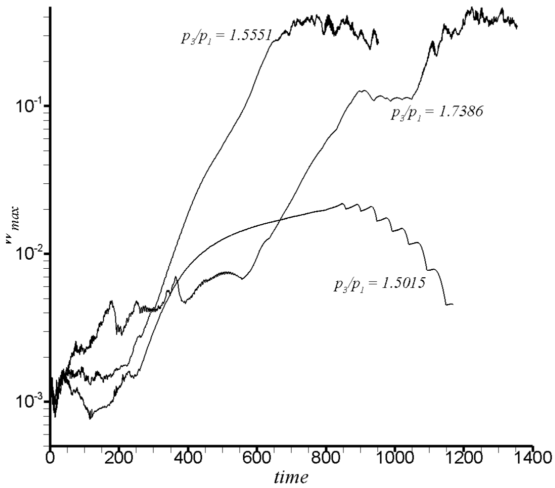


Figure 15: Temporal evolution of the maximum spanwise velocity ($w$) for the sbli cases with an initial random perturbations of $0.001u_\infty$.

vective amplification of upstream disturbances to a local absolute instability which leads to self-sustained turbulent flow in the absence of upstream disturbances.

This work was performed within the Long-Term Advanced Propulsion Concepts and Technologies project investigating high-speed air-breathing propulsion. LAPCAT, coordinated by ESA-ESTEC, is supported by the EU within the 6th Framework Programme Priority 1.4, Aeronautic and Space, Contract no.: AST4-CT-2005-012282. Further info on LAPCAT can be found on http://www.estec.esa.int/techresources/lapcat.

## References

Alam, M., Sandham, N. D., 2000, Direct Numerical Simulation of Short Laminar Separation Bubbles with Turbulent Reattachment, *J. Fluid. Mech.,* 410, 1-28.

Bogey, C., Bailly, C., 2004, A family of low dispersive and low dissipative explicit schemes for flow and noise computations, *J. Comput. Physics*, 194 (1): 194-214.

Chang, C. L., Malik, M. R., 1994, Oblique-mode breakdown and secondary instability in supersonic boundary layers,*J. Fluid. Mech.,* 273: 323-360.

Ducros, F., Ferrand, V., Nicoud, F., Weber, C., Darracq, D., Gacherieu, C., Poinsot, T., 1999, Large-eddy simulation of shock/turbulence interaction, *J. Computational Physics*, 152:517-549.

Hakkinen, R. J., Greber, I., Trilling, L., Abarnabel, S. S., 1959, The interaction of an oblique shock wave with a laminar boundary layer, *NASA CR 4274*.

Inagaki, M., Kondoh, T., Nagano, Y., 2005, A mixed-time-scale sgs model with fixed model-parameters for practical LES, *Transactions of the ASME, Journal of Fluids Engineering*, 127 (1),1-13.

Katzer, E., 1989, On the length scale of laminar shock/boundary-layer interaction, *J. Fluid Mech.*, 206: 477-496.

Krishnan, L., Sandham, N. D., 2004, Large eddy simulation of compressible turbulent spots, *Advances in Turbulence X*, H.I.Anderson and P.A.Krogstad(Eds),329,334.

Pagella, A., Babucke, A., Rist, U., 2004, Numerical investigations of small-amplitude disturbances in a boundary layer at Ma=4.8: compression corner vs. impinging shock wave, *Physics of Fluids*, 16 (7),2272-2281.

Sandham, N. D., Adams, N. A., Kleiser, L., 1994, Direct simulation of breakdown to turbulence following oblique instability waves in a supersonic boundary layer, *Direct and Large Eddy Simulation-I, P.R Voke et al. (Eds)*, 213-223.

Shen, Y., Wang, R., Liao, H., 2000, A new numerical study of the shock/boundary layer interaction, *Int. J. Numer. Methods in Fluids*, 33: 23-34.

Spalart, P. R., 1988, Direct simulation of turbulent boundary layer up to R = 1410, *J. Fluid. Mech.,* 187: 61-98.

Teramoto, S., 2005, Large eddy simulation of transitional boundary layer with impinging shock wave, *AIAA Journal*, 43 (11) : 2354-2363.

Theofilis, V., Hein, S., Dallmann, U., 2000, On the origins of unsteadiness and three-dimensionality in a laminar separation bubble, *Phil. Trans. R. Soc. Lond. A*, 358, 3229-3246.

Yao, Y., Krishnan, L., Sandham, N. D., Roberts, G. T., 2007, The effect of Mach number on unstable disturbances in shock/boundary-layer interactions, *Physics of Fluids*, 19, 054104.

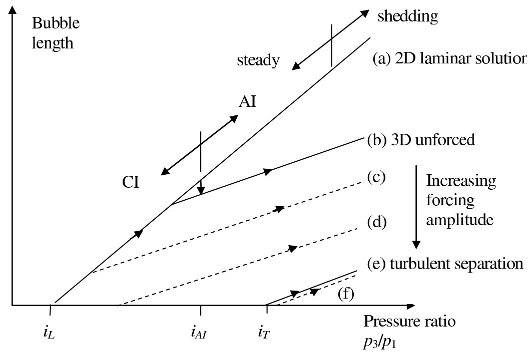


Figure 16: Separation bubble transition route.